increases progressively when the critical Mach number M_{crit} is exceeded. Wave drag can only be accurately computed by CFD methods. Considering the mixed flow in the transonic regime, an attempt to derive a meaningful analytical expression for wave drag is elusive. One will normally resort to experimental data to determine the aerodynamic coefficients accurately in this operating regime [6].

4.3 Subsonic Parasite and Induced Drag

Figure 4.1 decomposes total airplane drag alternatively into parasite drag and induced drag. The dotted connections indicate their relationship with the three physical mechanisms of drag and how they are affected by the most influential geometrical properties. The primary aim of this breakdown is to make a clear distinction between non-lifting and lifting bodies and to identify how their drag varies when the altitude and speed change. Many academic texts on aircraft performance apply to flight Mach numbers where the flow surrounding the aircraft does not contain regions of supersonic flow. In this flight regime, the only contribution to induced drag is vortex drag. In other words: induced drag and vortex drag are identical and – apart from Reynolds number effects – lift and drag coefficients depend only on the angle of attack.

Equations (4.2) and (4.4) show that, in steady level subsonic flight, only the variation of drag with the dynamic pressure q is relevant. Parasite and induced drag are closely related – but not exactly equal – to zero-lift drag and drag due to lift, respectively (Section 4.4). Basically, airplane parasite drag increases proportional to q, whereas induced drag varies inversely proportional to it.[4] In the condition of minimum total drag, parasite and induced drag are (approximately) equal. The variation of drag with flight conditions changes markedly at transonic speeds where parasite drag and induced drag are both affected by wave drag. The dominant parameter in this speed domain is the flight Mach number rather than the dynamic pressure (Section 4.4).

4.3.1 Parasite Drag

Acting on lifting as well as non-lifting airplane components, parasite drag D_p is decomposed into skin friction drag and a pressure drag term known as form drag. Parasite drag was traditionally known as profile drag, a term still in use for airfoils. At small incidences to low-speed flow, a relatively thin airfoil or a slender body of revolution has predominantly attached flow and form drag is an order of magnitude smaller than friction drag. Flow separation at high incidences increases the form drag of an airfoil considerably, whereas a swept-up aft fuselage can be a source of flow separation and vortical flow, causing significant form drag. Improvement of airfoil characteristics has been the subject of continuous R & D up to the present time. A classical overview of theory, test results and design for a large number of wing sections designed is published in NASA TR 824 – most of this work is available in [1]. Together with an abundance of information in [3], this source has formed a basis for low-speed airplane wing design up to the 1960s. Aerodynamic research during the 1970s and 1980s resulted in design methods based on CFD technology which enable the AD engineer to

[4]This property differs fundamentally from the air drag of non-lifting objects, such as ground vehicles, since they experience only parasite drag.

design airfoils specifically adapted for the application. Airframe manufacturers nowadays use high-fidelity aerodynamic design tools developed in-house.

Although laminar boundary layer friction is much lower, in practical cases the boundary layer of the airplane components is almost entirely turbulent. The flat plate analogy is widely used in conceptual design to compute the parasite drag of aircraft components from the friction drag of a smooth flat plate at zero incidence in turbulent flow. Classical equations used are the Von Kármán-Schoenherr formula

$$0.242 = \sqrt{C_{f_\mathrm{i}}} \log_{10} (C_{f_\mathrm{i}}\, Re_1) \tag{4.5}$$

or the Prandtl-Schlichting expression

$$C_{f_\mathrm{i}} = \frac{0.455}{(\log_{10} Re_1)^{2.58}} \tag{4.6}$$

with Reynolds numbers referred to the plate length. Since both equations apply to incompressible flow (index i) they must be corrected for reduced skin friction due to (subsonic) compressibility. Experimental data on the turbulent flat plate friction coefficient for Reynolds numbers between 10^6 and 10^8 adjusted to Mach 0.5 can be approximated as follows:

$$C_f = \frac{0.044}{Re_1^{1/6}} \tag{4.7}$$

The flat plate analogy derives the parasite drag area from

$$F_\mathrm{p} \stackrel{\mathrm{def}}{=} C_{D_\mathrm{p}} S = \Phi_\mathrm{f}\, C_f\, S_\mathrm{wet} \tag{4.8}$$

where C_f is the skin friction coefficient of a flat plate with the same wetted area S_wet and Reynolds number as the component.[5] Accounting for flow supervelocities and pressure drag, the form factor Φ_f is the ratio between the body's parasite drag and the skin friction drag of the equivalent plate. The parasite drag area of a body can be interpreted as the area of a hypothetical plate normal to the free stream, having a drag coefficient of 1.0 and the same parasite drag as the body. This parameter can be seen as a quantitative dimensional value expressing the parasite drag of an aircraft configuration. For instance, approximate values are $F_\mathrm{p} = 1.7$ m^2 for the Fokker 100 and $F_\mathrm{p} = 7.1$ m^2 for the B 747-100.

Design handbooks might suggest that the prediction method for the friction drag coefficient and the form factor is highly accurate. In reality, the assumption of a fully turbulent boundary layer is not necessarily correct whereas the seemingly unambiguous methods for computing form factors are actually based on a specific class of wing sections. One reason is that the only form factors present in most handbook methods is the thickness ratio and sweep angle for wings, and the fineness ratio for fuselages. As an alternative, Figure 4.2 compares non-lifting wings and fuselages by relating Φ_f to the ratio of frontal to wetted area. Due to the higher supervelocities along the wing surface, Φ_f is 15 to 25% higher compared to a fuselage. And since wings mostly have a (much) lower average Reynolds number, their C_f is at least

[5]The wetted (or exposed) area of a body is the external surface which is in contact with the airflow. See Appendix A.

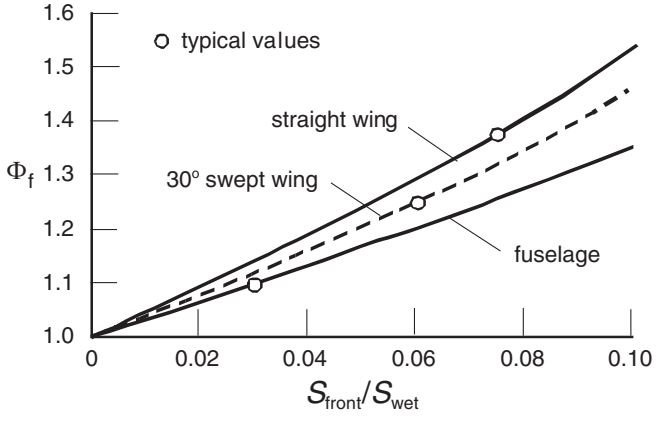

Figure 4.2 The form factor derived from experimental data

25% higher. Consequently, the wing's parasite drag area is significantly higher than that of a fuselage with the same wetted area. The discussion in Chapter 5 makes it clear that this observation is important when different airplane concepts are compared.

Aerodynamic design of a wing may require a more accurate drag prediction method than Equation (4.8). The parasite drag of a lifting surface is then computed by integrating the section profile drag for a number of airfoil sections along the span. Figure 4.3 shows how the section profile drag coefficient is affected by lift and camber. The drag variation with lift is related to flow supervelocities and boundary layer thickening at the trailing edge, rather than being induced by lift. Profile drag is minimal for the design lift coefficient c_{l_d} which is proportional to camber. For positive camber the minimum drag occurs for positive lift. The drag coefficient can be approximated for normal operating lift coefficients as follows:

$$c_{d_p} = (c_{d_p})_d\{1 + k_l(c_l - c_{l_d})^2\} \tag{4.9}$$

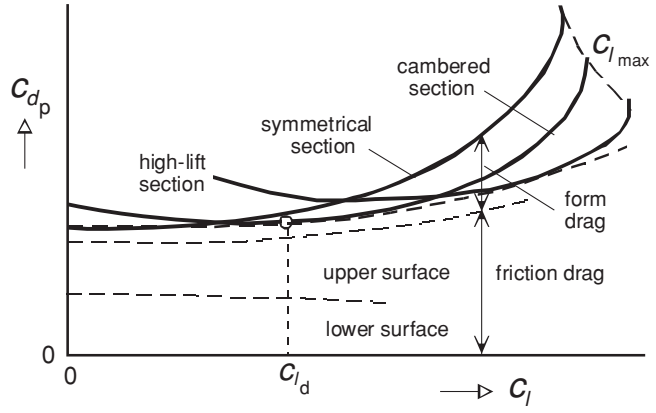

Figure 4.3 Section profile drag coefficient affected by camber and lift

The factor k_l depends on the section shape, in particular its thickness ratio. Equation (4.9) underestimates the drag at high incidences and loses its validity at the stall, when the lift actually decreases. Using the flat plate analogy should be obviated for low-drag wing sections designed for natural laminar flow (NLF), for which [23] and [32] are recommended. Another application of the flat plate analogy is wing area optimization. Variation of the design lift coefficient is then combined with wing section variation by selecting an optimum camber for each wing area. For this purpose the (dotted) enveloping curve in Figure 4.3 is used by inserting a modified (reduced) value $\overline{k}_l$ into the wing profile drag coefficient,

$$C_{D_p} = (C_{D_p})_{L=0}(1 + \overline{k}_l C_L^2) \tag{4.10}$$

4.3.2 Monoplane Induced Drag

The present section deals exclusively with flight at subcritical speed where induced drag is identical to vortex drag (Figure 4.1). Induced drag is generated predominantly by the wing, horizontal tail- and fore-plane surfaces. For an untwisted monoplane with elliptical chord and lift distribution, the classical result from the Lanchester/Prandtl lifting line theory is

$$D_i = \frac{L^2}{\pi q b_w^2} \quad \text{or} \quad C_{D_i} = \frac{C_L^2}{\pi A_w} \tag{4.11}$$

where b is the span measured in the lateral plane and $A_w = b_w^2/S_w$ denotes the aspect ratio. Equation (4.11) represents the theoretical minimum induced drag of a planar monoplane – it is considered as a reference for aerodynamic wing design. Since the lift distribution of the aircraft as a whole deviates from the elliptical, the induced drag coefficient is usually written as follows:

$$D_i = \frac{L^2}{\pi q b_w^2 e_v} \quad \text{or} \quad C_{D_i} = \frac{C_L^2}{\pi A_w e_v} \tag{4.12}$$

The span efficiency factor e_v depends on the distribution of lift along the span which is not necessarily independent of C_L. The theoretical span efficiency factor of a planar monoplane is less than or equal to 1.0. However, non-planar systems may achieve $e_v > 1.0$ and their induced drag can be significantly less than the reference given by Equation (4.11).

For a given lift distribution, the span efficiency factor of an symmetrical untwisted wing can be approximated in terms of the dimensionless lateral centre of lift located at η_c following [72]:

$$e_v = \{4.5(\pi \eta_c)^2 - 12\pi \eta_c + 9\}^{-1} \tag{4.13}$$

An elliptically loaded monoplane has the centre of lift at $\pi \eta_c = 4/3$ corresponding to $e_v = 1.0$. Dependent on the wing planform and the airplane's general arrangement, the span efficiency factor of a complete aircraft is (significantly) less than one. Figure 4.4 shows examples of an isolated wing as well as a wing in combination with a fuselage and/or engine nacelles. A well-designed trapezoidal wing achieves induced drag which is a few percentages above the theoretical minimum. The lift carry-over across the fuselage body is considered as reduced wing lift which increases induced drag in cruising flight by approximately 5%. Flow interaction

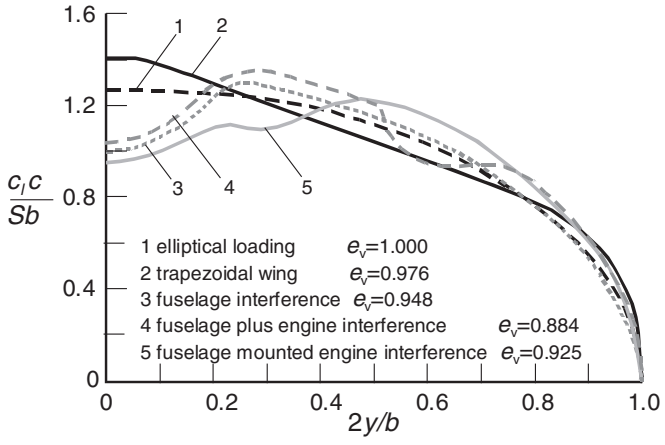

Figure 4.4 Lateral lift distribution and the span efficiency factor [38]

between wing and nacelles may lead to a significant modification of the lift distribution, with a drag penalty as indicated.

A twisted monoplane at zero lift carries positive lift over some parts of the span and negative lift over others – trailing vortices are then formed leading to induced drag. A wing with negative aerodynamic twist ('wash-out') at zero lift carries upward lift on the inboard wing and an equal downward lift on the outboard wing which reduces the induced drag for a selected range of lift coefficients. Compared to Equation (4.12), the following expression forms a more accurate representation:

$$C_{D_i} = \frac{(C_L - C_{L_x})^2}{\pi A_w e_x} + \left(C_{D_i}\right)_{\min} \tag{4.14}$$

where C_{L_x} and e_x are constants. Even though viscous drag is not included, Equation (4.14) describes an offset parabola which can be expanded into a three-term equation,

$$C_{D_i} = C_0 + C_1 C_L + C_2 C_L^2 \tag{4.15}$$

where C_0 and C_2 are positive and C_1 is (normally) negative. The ratio C_{D_i}/C_L is minimal for $C_L = \sqrt{C_0/C_2}$. Viscosity influences the lift distribution along the span and major interactions between viscous and vortex wake flows make an unambiguous decomposition of the associated drag components problematic. Incidentally, induced drag prediction for an airplane approaching the stall is not feasible – and unnecessary – in conceptual design.

4.3.3 Biplane Induced Drag

The induced drag analysis of a biplane system is complicated by the mutual interaction of the lifting surfaces. The aerodynamics of biplanes in combination with the general theorems of M. Munk [53] have been established in the form of Prandtl's classical biplane theory [54]. The

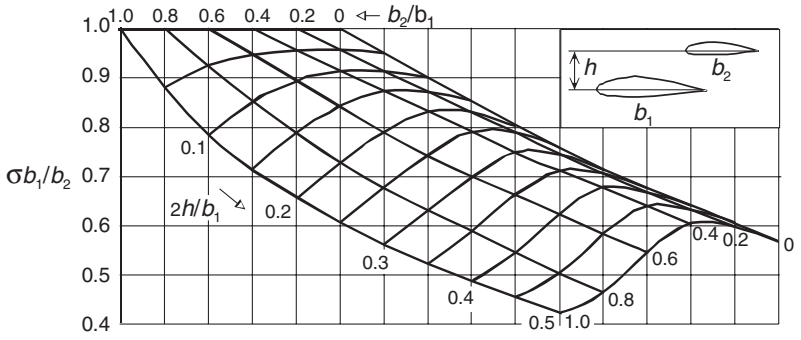

Figure 4.5 Prandtl's interference factor for biplanes

lift components of a biplane configuration are denoted L_1 acting on the forward wing with span b_1 and L_2 acting on the aft wing with span $b_2 < b_1$. Assuming that each wing has optimal (elliptical) loading, Prandtl obtained the total induced drag from the self-induced vortex drag of both wings in isolation according to Equation (4.11) with a drag increment caused by the mutual interaction between the two wings, resulting in

$$D_{\mathrm{i}} = \frac{1}{\pi q}\left\{\frac{L_1^2}{b_1^2} + 2\sigma\frac{L_1}{b_1}\frac{L_2}{b_2} + \frac{L_2^2}{b_2^2}\right\} \tag{4.16}$$

The interference factor σ, depicted in Figure 4.5, depends on the span ratio b_2/b_1 and on the gap h; that is, the vertical displacement between the wings. The equation approximating Prandtl's interference factor proposed by Laitone [59],

$$\sigma b_1/b_2 = 1 - \{1 + (b_1/2h)^2\}^{-1/2} \tag{4.17}$$

has an inaccuracy of less than 2% for $b_2/b_1 < 0.3$.

When Equation (4.16) is applied to a non-staggered biplane consisting of two wings with equal span b, it is readily found that minimum induced drag amounts to

$$(D_{\mathrm{i}})_{\min} = \frac{L}{\pi q\, b^2}\,\frac{1+\sigma}{2} \quad \text{for} \quad L_1 = L_2 = \frac{1}{2}L \tag{4.18}$$

For instance, if the two wings have a vertical displacement of 20% span, Prandtl's interference factor amounts to $\sigma = 0.485$ which yields a span efficiency factor$e_{\mathrm{v}} = 1.35$. Consequently, the biplane's induced drag is 26% less compared to a monoplane with the same lift and span. Munk's stagger theorem states that the total induced drag of a biplane system is unaltered if any of the lifting surfaces are moved in the direction of motion, provided the lateral lift distribution on each surface is constant. This principle is applied to a tandem wing configuration which features two highly staggered wings of equal span at the airplane's front and rear end. The condition of elliptic loading on both lifting surfaces is only satisfied for $b_1 > b_2$ which makes the biplane theory applicable to a wing-and-tail configuration with arbitrary stagger.

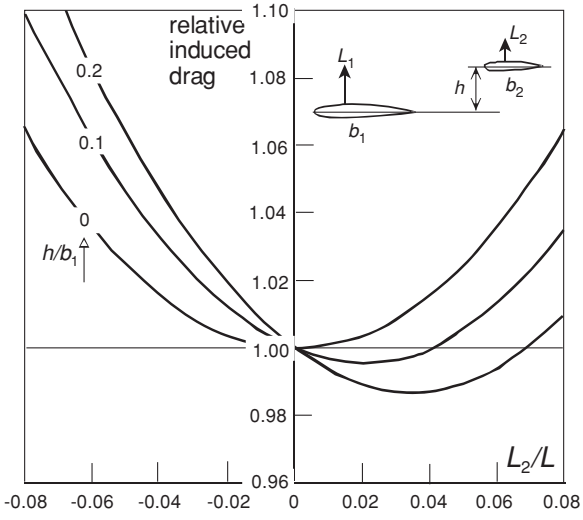

Figure 4.6 Induced drag of a wing-and-tail combination with $b_2/b_1 = 0.3$

The nose-plane of a canard configuration has a smaller span than the wing and its trailing vortex field causes the wing lift distribution to be heavily distorted relative to the elliptic loading. For this configuration Munk's stagger theorem is invalid, especially for a small vertical displacement between the two planes. Butler [64] and Kroo [63] demonstrated that the interference between the nose-plane and the wing reduces the induced drag of this configuration relative to classical biplane theory. They assumed an elliptical lift distribution on the nose-plane and optimized the main wing lift distribution immersed in the nose-plane's vortex field. The minimum total induced drag is summarized in a modified biplane equation,

$$D_{\mathrm{i}} = \frac{1}{\pi q}\left\{\sigma_{\mathrm{c}}\frac{L_1^2}{b_1^2} + 2\sigma\frac{L_1}{b_1}\frac{L_2}{b_2} + \frac{L_2^2}{b_2^2}\right\} \tag{4.19}$$

with values of σ_{c} obtained from [63]. Equation (4.19) is applicable to a wing-and-tail combination ($b_1 > b_2$) with $\sigma_{\mathrm{c}} = 1$ as well as to a canard airplane ($b_1 < b_2$) with $0 < \sigma_{\mathrm{c}} < 1$.

As an example, Figure 4.6 depicts the induced drag of a wing-and-tail combination compared to the case when all the lift is carried by the wing. For a tail located in the wing plane ($h = 0$), there is a drag penalty if the tail load is upward or downward.[6] A high-set stabilizer may generate a modest induced drag reduction if it has an upward lift of about 3% of the total lift; however, even a small tail download causes a considerable drag penalty. Due to the high nose-plane lift inherent to a typical canard configuration its induced drag penalty is relatively high, especially if the classical biplane theory ($\sigma_{\mathrm{c}} = 1$) were used. Figure 4.7 illustrates that applying a realistic $\sigma_{\mathrm{c}} = 0.65$ reduces the drag penalty by more than 50%. It can safely be concluded that the lowest vortex drag of a canard-and-wing combination is obtained when the wing, with its large span, carries the highest possible fraction of the total lift.

[6]For a given flight condition, the tail load is determined by the airplane's centre of gravity (CG) location. The tailplane of a transport aircraft mostly carries negative lift.

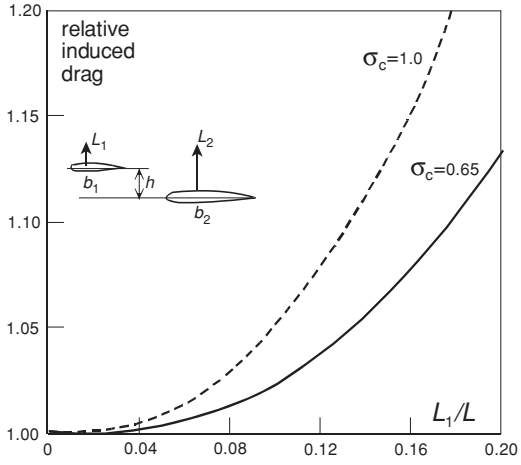

Figure 4.7 Induced drag of a canard airplane with $b_1/b_2 = 0.4$

4.3.4 Multiplane and Boxplane Induced Drag

The induced drag of an optimally loaded triplane is smaller than the minimum induced drag of a biplane with equal span and height. Induced drag approaches a lower limit when the number of multiplanes tends to infinity. However, L. Prandtl has proved that the minimum induced drag of a system of identical parallel lifting surfaces is equal to that of a closed lifting system consisting of a biplane interconnected by tip planes. This principle is materialized in the boxplane concept consisting of a biplane with wings of equal span connected at their tips by vertical planes. The front view of a boxplane in Figure 4.8 (a) shows that the horizontal surfaces carry the same lift, with an optimal lift distribution consisting of a constant part and an elliptical one. The circulation on the vertical planes is zero at their midpoint with equal

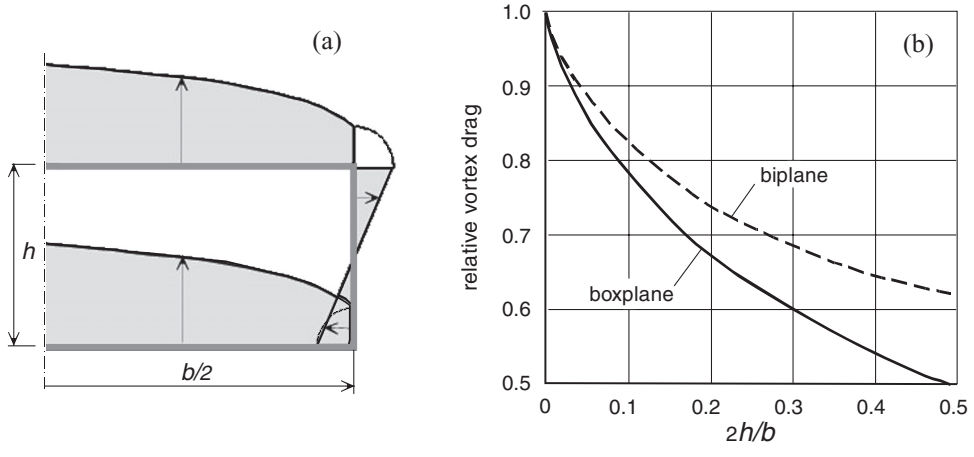

Figure 4.8 Obtainable vortex drag reduction of biplanes and boxplanes. (a) Optimum lift distribution of a boxplane. (b) Minimum vortex drag compared to a monoplane